First Principles Study of Ferroelastic Twins in Halide Perovskites

Andrew R. Warwick,[†] Jorge Íñiguez,[‡,¶] Peter D. Haynes,[†] and Nicholas C. Bristowe[*,§,†]

†*Department of Materials, Imperial College London, London SW7 2AZ, United Kingdom*

‡*Materials Research and Technology Department, Luxembourg Institute of Science and Technology, 5 avenue des Hauts-Fourneaux, 4362 Esch/Alzette, Luxembourg*

¶*Physics and Materials Science Research Unit, University of Luxembourg, 41 Rue du Brill, L-4422 Belvaux, Luxembourg*

§*School of Physical Sciences, University of Kent, Canterbury,CT2 7NH, United Kingdom*

E-mail: N.C.Bristowe@kent.ac.uk

Abstract

We present an *ab initio* simulation of 90° ferroelastic twins that were recently observed in methyl ammonium lead iodide. There are two inequivalent types of 90° walls that we calculate to act as either electron or hole sinks which leads us to propose a mechanism for enhancing charge carrier separation in photovoltaic devices. Despite separating non-polar domains, we show these walls to have a substantial in-plane polarization of ~ 6 μC cm^{-2}, due in part to flexoelectricity. We suggest this in turn could allow for the photoferroic effect and create efficient pathways for photocurrents within the wall.

Graphical TOC Entry

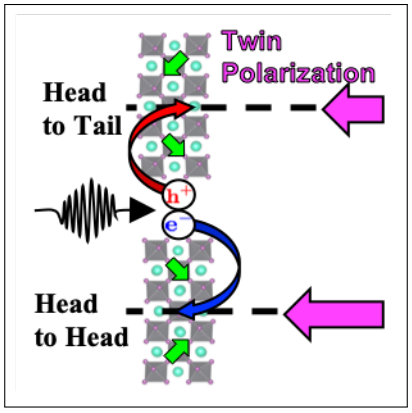

The synthesis of a hybrid organic-inorganic halide perovskite ('HOIP') solar cell was first reported in 2009.[1] Since then, the power conversion efficiencies (PCE) of these devices have climbed rapidly from 14.3% to 23.7%.[2] A wide range of materials, in particular methylammonium lead iodide ($CH_3NH_3PbI_3$, 'MAPI'), have been considered to investigate this class of photovoltaic devices. Key issues regarding the stability and efficiency of these materials are an ongoing area of research (*cf.* reviews[3,4] and references therein), not least of which is the origin of their high PCE. In this context, an important open question is whether MAPI is ferroelectric[5] and, secondly by extension, how the photoferroic effect[6–8] might play a role in the reported PCEs. As of yet, there is no clear consensus on the former issue.[9–15] In addition to multiple related studies on the bulk material, there have been a number of publications on planar defects such as grain boundaries and domain walls which we briefly summarise here (more detailed reviews can be found in[16,17]).

At a defect boundary, properties not present in the bulk may emerge at the interface itself, chiefly due to the local structural distortion. For instance, a bulk property may change orientation across the boundary and thus some components will locally vanish or be enhanced. Hence, physics that is ordinarily suppressed in the bulk may manifest at the wall. Theoretical studies on grain boundaries[18–22] and ferroelectric domain walls[9,23,24] have proposed a variety of ways in which these types of planar defects may influence the electronic properties of HOIPs. Some first–principles simulations suggest that the presence of grain boundaries is not detrimental to photovoltaic performance.[19,21,22] Conversely, experimental evidence indicates charge carrier recombination is enhanced at these defects.[25] It has been proposed that ferroelectric domain walls ('twins') can be formed via interfacing polar domains in which the methyl ammonium (MA) molecular dipoles are aligned. Calculations on these twins indicate beneficial effects such as locally diminished band gaps[23,24] or enhanced charge carrier diffusion lengths.[9]

Recently, ferro*elastic* twins in MAPI were observed at room temperature and their structure has been determined.[26–28] We emphasise that these types of defect are distinct from the

aforementioned grain boundaries and ferroelectric twins. Ferroelastic domain walls separate domains with different strain states. Unlike a general grain boundary, the domains are crystallographically related.[29] In contrast to ferroelectric twins, these domains can be non-polar (which may be the case in MAPI). Nonetheless, to the best of our knowledge, an *ab initio* simulation of the ferroelastic twins observed and described here has not been carried out.

Here, we report a density-functional theory simulation of 90° ferroelastic twins characterised in MAPI.[26–28] We find the walls to be thin, polar and have a low formation energy. The effect of these properties on the photovoltaic performance of halide perovskites is discussed in addition to possible avenues for domain-wall engineering such devices.

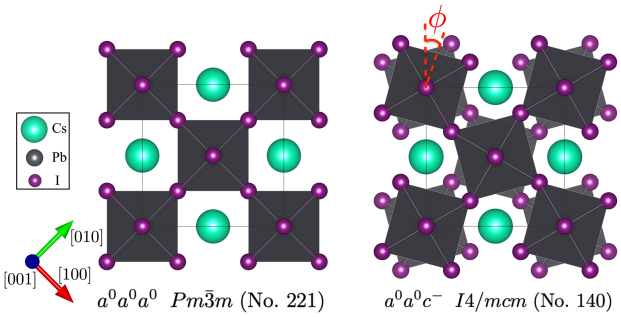

Figure 1: Illustration of the cubic $Pm\bar{3}m$ and tetragonal $I4/mcm$ phases of $CsPbI_3$. The $I4/mcm$ phase is characterised by octahedral tilting about one axis. The octahedra maintain corner connectivity and tilt about the [001] direction (pointing out of the page) through an angle ϕ in opposite senses along (001) planes as denoted by Glazer's notation $a^0a^0c^-$.

There are obvious technical challenges to account for the dynamic ordering of MA molecules in a zero kelvin calculation. Hence we studied these walls in $CsPbI_3$, the Cs atom having a similar effective size to the MA molecule.[30] Furthermore, the valence and conduction band edges are known to be mainly dominated by Pb and I states.[31] Hence, we expect MAPI twins to display the properties presented here with additional physics arising from the organic molecule. In addition, the use of $CsPbI_3$ in synthesising photovoltaic devices[32] and doping MAPI with Cs to improve PCE[33] make this topical in its own right.

MAPI and $CsPbI_3$ adopt the perovskite structure of corner-sharing I_6 octahedra with MA^+/Cs^+ and Pb^{2+} cubic sub–lattices. We studied the room temperature tetragonal phase

of MAPI with $CsPbI_3$ where the I_6 octahedra tilt in antiphase with angle ϕ along one tetrad axis (shown in Fig. 1). The phase has space group $I4/mcm$ (No. 140)[34] with Glazer tilt pattern $a^0a^0c^-$ (indicating no octahedral tilts about [100] and [010] directions and an antiphase tilt about the [001] axis[35]). This single domain state may be characterised by a pseudovector $\boldsymbol{\phi}$ parallel to the tilt axis and whose magnitude is equal to the tilt angle ϕ. Note that the symmetry of this anti-phase tilt makes the $I4/mcm$ space group necessarily non-polar. Due to the spontaneous strain induced by ϕ, such a state is termed improper ferroelastic.

The twins characterised by Rothmann *et al.*[26] are planar interfaces joining two domains whose tilt axes meet at 90°. Figure 2a) shows two atomic structures consistent with these observed twins. Directions perpendicular and parallel to the planar interface are labelled by unit vectors $\hat{\mathbf{s}}$ and $\hat{\mathbf{r}}$ respectively. In fact, it can be shown that these are the only mechanically compatible 90° twins[29] i.e. interfaces that do not introduce additional strains and stresses to this system. Both twins in Fig. 2 may be characterised by the relative orientation of tilt pseudovectors across the wall's center. Following standard terminology,[36] these are called 'head to tail' (HT) or 'head to head' (HH).

The twins were simulated with periodic boundary conditions in VASP 5.4.4[37–40] using the PBEsol exchange-correlation functional.[41] Valence electron configurations $6s^1$, $6s^2p^2$ and $5s^2p^5$ were employed for Cs, Pb and I respectively with the supplied Projector-Augmented-Wave pseudopotentials generated in 2002.[37,39,42,43] We used supercells containing 200 atoms, the centers of which are shown in Fig. 2a), such that the cell contained two walls (one at the center and another shared at the edges) yet was sufficiently large to recover the bulk properties between both walls. With an energy cutoff of 500 eV for the plane-wave basis and a $4 \times 5 \times 1$ Monkhorst-Pack grid,[44] both supercells were relaxed such that the maximum force on any atom is less than 10 meV $Å^{-1}$.

We determined the formation energies of the twin boundaries to be $4.4\,\mathrm{mJ\,m^{-2}}$ and $-1.2\,\mathrm{mJ\,m^{-2}}$ for the HT and HH walls respectively (details are given in the Supporting

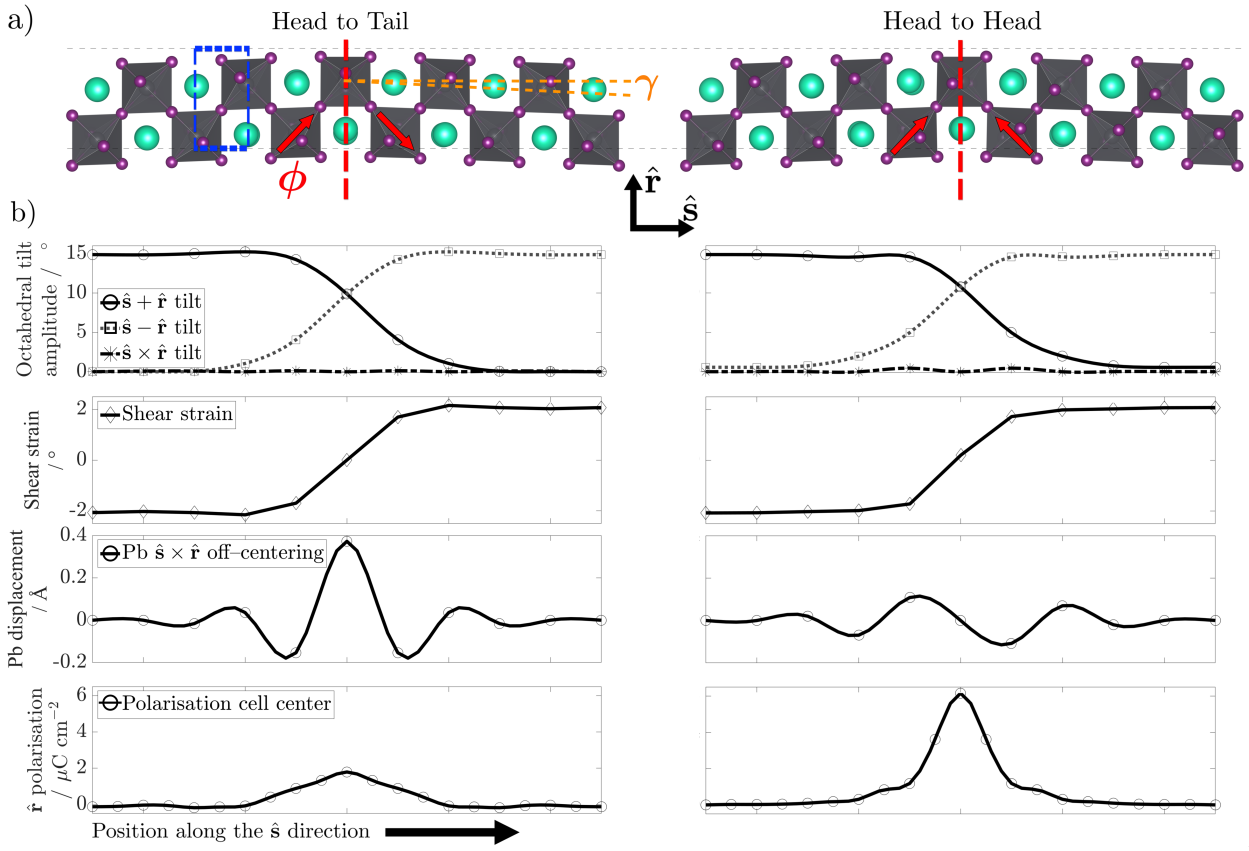

Figure 2: a) Structure and b) properties of the HT (left) and HH (right) twins. The plots are (from top to bottom) profiles of tilt amplitude, an estimate of shear strain, Pb^{2+} cation $\hat{\mathbf{s}} \times \hat{\mathbf{r}}$ off–centerings and the in–plane $\hat{\mathbf{r}}$ polarization component (as obtained from the calculated displacements and Born effective charges (BEC)). For both walls, the x–axis marks units of distance along $\hat{\mathbf{s}}$ and is plotted to scale with the respective atomic configuration above. Tilt pseudovectors and the wall central plane are marked by red arrows (labelled $\boldsymbol{\phi}$) and a vertical dashed line in both structural schematics. Shear strain was quantified by the angle γ coloured orange in a). Pb off-centerings are plotted for octhedra visible in the plane of this page; for the adjacent plane of octhedra below/above along the $\hat{\mathbf{s}} \times \hat{\mathbf{r}}$ direction, the Pb off-centerings are in antiphase. The polarizations were calculated at cells indicated by the dashed blue box in the HT schematic.

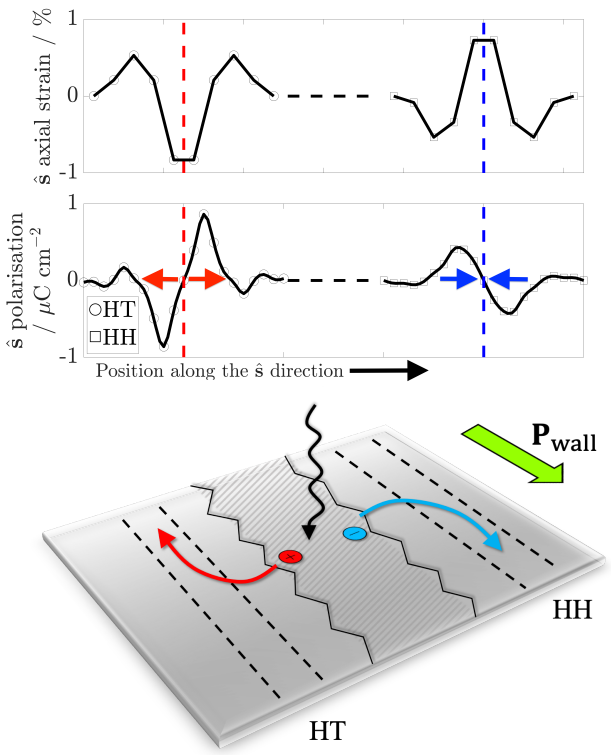

Figure 3: HT (left) and HH (right) axial $\hat{\mathbf{s}}$ strain (top plot) and $\hat{\mathbf{s}}$ component of polarization $\mathbf{P}$ (bottom plot) as a function of position along the boundary normal $\hat{\mathbf{s}}$ implying their role as hole and electron sinks respectively. Red and blue arrows represent the direction of $\hat{\mathbf{s}}$ polarization components local to the wall (not to scale). A mechanism for enhancing charge carrier mobility and delaying recombination rate is proposed in the bottom panel where HT and HH walls with parallel polarizations are engineered to be brought within the vicinity of each other.

Information). The negative HH formation energy was found to arise from the octahedral tilt pattern across the wall. Between both single antiphase tilt I4/mcm $a^0a^0c^-$ domains, there is an intermediate structure characterised by two antiphase axes of different tilt amplitudes (*cf.* Fig. 2). This phase is of space group $C2/m$ with Glazer notation $a^0b^-c^-$. Unusually, the $C2/m$ phase was found to be more stable than $I4/mcm$ in our PBEsol calculations, which correspond to the limit of 0 K. We arrived at the same conclusion using the PBE functional and for different $APbX_3$ chemistries where A = Fr, Rb and X = I, F. Nonetheless, these are small formation energies. Hence, as has been observed experimentally,[26–28] we expect these walls to appear frequently.

The wall thicknesses were extracted from the change in octahedral tilts across the wall.

Figure 2 shows plots of the magnitude of the cubic tilt vectors $\boldsymbol{\phi}$ with respect to position along the $\hat{\mathbf{s}}$ direction. Fitting a hyperbolic tangent function $\sim \phi_0 \tanh(x/\delta)$,[29] where ϕ_0, x and δ correspond to the bulk tilt amplitude, position along $\hat{\mathbf{s}}$ and the fitting parameter respectively, yields thicknesses of $2\delta \sim 1$ nm for both walls, indicating that they are thin. For comparison, in the prototypical $I4/mcm$ oxide perovskite $SrTiO_3$, the same wall geometries were calculated to have much larger thicknesses of 7-8 nm.[36] Our results imply that any emergent phenomena at the walls could be highly localised. Furthermore, these boundaries are likely to be relatively immobile in response to an external stress,[45] which would help prevent wall annihilation.

We found both ferroelastic twins to be polar; a result that has not been discussed in observations of these twins.[17,26–28,46–49] The layer-by-layer polarization $\mathbf{P}$ was determined using Born effective charges computed in the centrosymmetric $Pm\bar{3}m$ structure (details are given in the Supporting Information). The $\hat{\mathbf{s}} \times \hat{\mathbf{r}}$ and $\hat{\mathbf{s}}$ components were antipolar and hence contributed no net polarization across the wall. Conversely, the $\hat{\mathbf{r}}$ component of $\mathbf{P}$ is plotted in Fig. 2, yielding a relatively large net polarization peaking at ~ 1.8 and 6 μC cm^{-2} in the HT and HH walls respectively. The same domain wall geometries in $SrTiO_3$ have been calculated to yield polarizations up to 0.2 μC cm^{-2}.[36] We found this to be signficantly driven by Cs-cation off-centering in the HH wall, as opposed to that in the HT wall where the main contribution is from the larger Pb-cation Born effective charge. In the hybrid organic-inorganic system, we could expect the dipole moment of MA to either enhance or diminish this contribution to the polarization. Evidently, this issue requires further investigation. However in any case, the in-plane polarization must remain non-zero whether the A-site is occupied by an MA molecule or Cs cation due to the wall symmetry. To be more specific, even if the MA molecules can oscillate and are therefore partly disordered,[50] since inversion symmetry is broken in the wall region, the molecules are subject to an effective electric field that, on average, will yield a non-zero polarization.

In any case, we note that ferroelastic boundaries are necessarily polar.[29] One may un-

derstand this as follows. The juxtaposition of strain states from both domains introduces a strain gradient across the wall. In ferroelastic twins, the spatial integral of this gradient is non–zero. This necessarily induces a flexoelectric effect (a coupling between strain gradient and electric polarization) that breaks inversion symmetry and allows for a net polarization.[36] One may estimate this coupling to be particularly pronounced in these walls as shown in Fig. 2b) by the large gradient in shear strain. It can be shown that the emergent polarization at the wall is in-plane, corresponding to the $\hat{\mathbf{r}}$ direction in these HH and HT twins as confirmed by our results.

Although these walls are polar, this is only a necessary but not sufficient condition for ferroelectricity. To shed some light on this issue, we note that Schiaffino and Stengel have derived a Landau-like expansion of the potential energy landscape for the same wall geometries.[36] They identified three 'improper' terms that are linear in $\mathbf{P}$ and arise due to the walls' structure. These terms describe couplings of $\mathbf{P}$ with strain gradients ('flexoelectric'), tilts and tilt gradients ('rotopolar') in addition to a term coupling $\mathbf{P}$ with anti-polar B-cation off-centerings and tilts. These tilt, shear strain and Pb $\hat{\mathbf{s}} \times \hat{\mathbf{r}}$ displacement profiles are plotted in Fig. 2. For an improper term to remain invariant under $\mathbf{P}$ reversal, the sign of precisely one of the other terms in the coupling must also change. Due to the wall geometry, that appears unlikely to be possible and hence we would not expect this improper polarization to be switchable. However, from computing phonon modes of the intermediate two (anti-phase) tilt system at the wall, we found this phase to contain an unstable polar mode. This indicates a double well polarization for $CsPbI_3$, even after normalization with the competitive bi-quadratic coupling term from the tilts, and hence the possibility of an additional proper and switchable component to the polarization. It is possible that a combination of these proper and improper polarizations may allow for the walls to be ferroelectric through the presence of multiple metastable polar states. Nonetheless, we note that the aforementioned flexoelectricity and the photoferroic effect could play an important role in the photovoltaic performance of HOIPs, irrespective of whether or not $\mathbf{P}$ is switchable.[51] The notion that

strain and strain gradients bring about such effects in MAPI has been hypothesised [52,53] and, in addition to the characterization of these twins, Liu *et al.* [27,28] have imaged ionic segregation across the twin boundary which they attribute to the variation of strain.

Figure 3 shows an estimate for axial strain perpendicular to the wall (details are given in the Supporting Information) and the out-of-plane $\hat{\mathbf{s}}$ components of $\mathbf{P}$ as a function of distance along the $\hat{\mathbf{s}}$ direction. The character of these polarization components at the interface suggests that the HT and HH walls act as hole and electron sinks respectively. We propose that this could allow for the interfaces to be engineered as pathways that enhancing electron/hole mobility. Consider a configuration where HT and HH walls with parallel polarizations are brought close to each other (*n.b.* even a sequence of antiparallel polarizations from both types of wall may yield a non–zero macroscopic polarization [36]). Upon photoexcitation, an electron-hole pair may be separated into walls that act as their respective sinks, confining the charge carriers to the boundary and delaying recombination. The in-plane wall polarizations then would enhance electron/hole mobility along the walls, similar to the ferroelectric highways depicted by Frost *et al.* [9] In these ferroelastic twins, their experimental observation [26] shows these walls to span over large distances and be a bulk phenomenon which may further support the proposed mechanism. The topic of domain boundary engineering is an important point of future work. We note various papers on this topic [54,55] in addition to research indicating the possibility of reliably growing well ordered domain structures. [47,56,57]

From the projected density of states we found the band gap at the walls and in bulk to be largely similar. However, in general this may be an additional effect at different types of domain walls, which will be a point of future investigation.

In this article, we have presented an *ab initio* study of ferroelastic 90° $CsPbI_3$ twins. Our study serves as a model for ferroelastic twins recently observed in MAPI that have the same structure [26] as those considered here. Both types of twins, HH and HT, were found to have a low formation energy, small thickness and a sizeable in-plane polarization of $\sim 6\ \mu\text{C cm}^{-2}$ despite separating non-polar domains. Due to the structure of both walls,

this in-plane polarization is necessarily non-zero. Whilst providing insight to the intrinsic properties of MAPI, these results should also contribute to the ongoing debate on whether MAPI is ferroelectric. Potential avenues for enhancing photovoltaic performance via domain wall engineering have been discussed with a mechanism proposed for delaying recombination rates and enhancing charge carrier mobility. We hope to motivate further investigation into these structures (*e.g.* by measuring the in-plane polarization at each wall) and their role in the performance of hybrid organic-inorganic halide perovskite solar cells.

Acknowledgement

We are grateful for the computational resources provided by the Imperial College Research Computing Service and the UK Materials and Molecular Modelling Hub, which is partially funded by EPSRC (EP/P020194/1). This work has been supported by the EPSRC Centre for Doctoral Training on Theory and Simulation of Materials (TSM-CDT, grant ref. EP/L015579/1). J.Í. thanks the support of the Luxembourg National Research Fund (Grant FNR/C15/MS/10458889 NEWALLS). Structural schematics in Fig. 1 & 2 were generated using the visualization software VESTA 3.[58]

Supporting Information Available

In addition to the input and output files for our calculations, the methods for computing domain wall energy, Born Effective Charge polarization and axial strain are given in the supporting information.

This material is available free of charge via the Internet at `http://pubs.acs.org/`.

References

(1) Kojima, A.; Teshima, K.; Shirai, Y.; Miyasaka, T. Organometal Halide Perovskites as Visible-Light Sensitizers for Photovoltaic Cells. *J. Am. Chem. Soc.* **2009**, *131*, 6050–6051.

(2) *Best Research Cell Efficiencies, NREL*; National Renewable Energy Laboratory: Golden, CO, 2019.

(3) Bhatt, M. D.; Lee, J. S. Current Drogress and Scientific Challenges in the Advancement of Organic–Inorganic Lead Halide Perovskite Solar Cells. *New J. Chem.* **2017**, *41*, 10508–10527.

(4) Huang, J.; Yuan, Y.; Shao, Y.; Yan, Y. Understanding the Physical Properties of Hybrid Perovskites for Photovoltaic Applications. *Nat. Rev. Mater.* **2017**, *2*, 17042.

(5) Garten, L. M.; Moore, D. T.; Nanayakkara, S. U.; Dwaraknath, S.; Schulz, P.; Wands, J.; Rockett, A.; Newell, B.; Persson, K. A.; Trolier-McKinstry, S. et al. The Existence and Impact of Persistent Ferroelectric Domains in MAPbI3. *Sci. Adv.* **2019**, *5*, eaas9311.

(6) Fridkin, V. M. *Photoferroelectrics (Springer Series in Solid State Science)*; Springer-Verlag, Berlin: Berlin, Germany, 1979; Vol. 9.

(7) Sturman, P. J.; Fridkin, V. M. *Photovoltaic and Photo-Refractive Effects in Noncentrosymmetric Materials*; Taylor & Francis Ltd: London, U.K., 1992; Vol. 8.

(8) Butler, K. T.; Frost, J. M.; Walsh, A. Ferroelectric Materials for Solar Energy Conversion: Photoferroics Revisited. *Energy Environ. Sci.* **2015**, *8*, 838–848.

(9) Frost, J. M.; Butler, K. T.; Brivio, F.; Hendon, C. H.; van Schilfgaarde, M.; Walsh, A. Atomistic Origins of High-Performance in Hybrid Halide Perovskite Solar Cells. *Nano Lett.* **2014**, *14*, 2584–2590.

(10) Kutes, Y.; Ye, L.; Zhou, Y.; Pang, S.; Huey, B. D.; Padture, N. P. Direct Observation of Ferroelectric Domains in Solution-Processed CH3NH3PbI3 Perovskite Thin Films. *J. Phys. Chem. Lett.* **2014**, *5*, 3335–3339.

(11) Fan, Z.; Xiao, J.; Sun, K.; Chen, L.; Hu, Y.; Ouyang, J.; Ong, K. P.; Zeng, K.; Wang, J. Ferroelectricity of CH3NH3PbI3 Perovskite. *J. Phys. Chem. Lett.* **2015**, *6*, 1155–1161.

(12) G, S.; Mahale, P.; Kore, B. P.; Mukherjee, S.; Pavan, M. S.; De, C.; Ghara, S.; Sundaresan, A.; Pandey, A.; Guru Row, T. N. et al. Is CH3NH3PbI3 Polar? *J. Phys. Chem. Lett.* **2016**, *7*, 2412–2419.

(13) Kim, Y.-J.; Dang, T.-V.; Choi, H.-J.; Park, B.-J.; Eom, J.-H.; Song, H.-A.; Seol, D.; Kim, Y.; Shin, S.-H.; Nah, J. et al. Piezoelectric Properties of CH3NH3PbI3 Perovskite Thin Films and their Applications in Piezoelectric Generators. *J. Mater. Chem. A* **2016**, *4*, 756–763.

(14) Rakita, Y.; Bar-Elli, O.; Meirzadeh, E.; Kaslasi, H.; Peleg, Y.; Hodes, G.; Lubomirsky, I.; Oron, D.; Ehre, D.; Cahen, D. Tetragonal CH3NH3PbI3 is Ferroelectric. *Proc. Natl. Acad. Sci. U. S. A.* **2017**, *114*, E5504–E5512.

(15) Hoque, M. N. F.; Yang, M.; Li, Z.; Islam, N.; Pan, X.; Zhu, K.; Fan, Z. Polarization and Dielectric Study of Methylammonium Lead Iodide Thin Film to Reveal its Nonferroelectric Nature under Solar Cell Operating Conditions. *ACS Energy Lett.* **2016**, *1*, 142–149.

(16) Whalley, L. D.; Frost, J. M.; Jung, Y.-K.; Walsh, A. Perspective: Theory and Simulation of Hybrid Halide Perovskites. *J. Chem. Phys.* **2017**, *146*, 220901.

(17) Liu, W.; Liu, Y.; Wang, J.; Wu, C.; Liu, C.; Xiao, L.; Chen, Z.; Wang, S.; Gong, Q. Twin Domains in Organometallic Halide Perovskite Thin-Films. *Crystals* **2018**, *8*.

(18) Shan, W.; Saidi, W. A. Segregation of Native Defects to the Grain Boundaries in Methylammonium Lead Iodide Perovskite. *J. Phys. Chem. Lett.* **2017**, *8*, 5935–5942.

(19) Yin, W.-J.; Shi, T.; Yan, Y. Unique Properties of Halide Perovskites as Possible Origins of the Superior Solar Cell Performance. *Adv. Mater.* **2014**, *26*, 4653–4658.

(20) McKenna, K. P. Electronic Properties of {111} Twin Boundaries in a Mixed-Ion Lead Halide Perovskite Solar Absorber. *ACS Energy Lett.* **2018**, *3*, 2663–2668.

(21) Guo, Y.; Wang, Q.; Saidi, W. A. Structural Stabilities and Electronic Properties of High-Angle Grain Boundaries in Perovskite Cesium Lead Halides. *J. Phys. Chem. C* **2017**, *121*, 1715–1722.

(22) Yin, W.-J.; Chen, H.; Shi, T.; Wei, S.-H.; Yan, Y. Origin of High Electronic Quality in Structurally Disordered CH3NH3PbI3 and the Passivation Effect of Cl and O at Grain Boundaries. *Adv. Electron. Mater.* **2015**, *1*, 1500044.

(23) Liu, S.; Zheng, F.; Koocher, N. Z.; Takenaka, H.; Wang, F.; Rappe, A. M. Ferroelectric Domain Wall Induced Band Gap Reduction and Charge Separation in Organometal Halide Perovskites. *J. Phys. Chem. Lett.* **2015**, *6*, 693–699.

(24) Chen, L.; Paillard, C.; Zhao, H. J.; Íñiguez, J.; Yang, Y.; Bellaiche, L. Tailoring Properties of Hybrid Perovskites by Domain-Width Engineering with Charged Walls. *npj Comput. Mater.* **2018**, *4*, 75.

(25) Bischak, C. G.; Sanehira, E. M.; Precht, J. T.; Luther, J. M.; Ginsberg, N. S. Heterogeneous Charge Carrier Dynamics in Organic–Inorganic Hybrid Materials: Nanoscale Lateral and Depth-Dependent Variation of Recombination Rates in Methylammonium Lead Halide Perovskite Thin Films. *Nano Lett.* **2015**, *15*, 4799–4807.

(26) Rothmann, M. U.; Li, W.; Zhu, Y.; Bach, U.; Spiccia, L.; Etheridge, J.; Cheng, Y.-

B. Direct Observation of Intrinsic Twin Domains in Tetragonal CH3NH3PbI3. *Nat. Commun.* **2017**, *8*, 14547.

(27) Liu, Y.; Collins, L.; Belianinov, A.; Neumayer, S. M.; Ievlev, A. V.; Ahmadi, M.; Xiao, K.; Retterer, S. T.; Jesse, S.; Kalinin, S. V. et al. Dynamic Behavior of CH3NH3PbI3 Perovskite Twin Domains. *Appl. Phys. Lett.* **2018**, *113*, 072102.

(28) Liu, Y.; Collins, L.; Proksch, R.; Kim, S.; Watson, B. R.; Doughty, B.; Calhoun, T. R.; Ahmadi, M.; Ievlev, A. V.; Jesse, S. et al. Chemical Nature of Ferroelastic Twin Domains in CH3NH3PbI3 Perovskite. *Nat. Mater.* **2018**, *17*, 1013–1019.

(29) *International Tables for Crystallography*, 2nd ed.; John Wiley & Sons, Ltd.: New Jersey, U.S.A., Vol. D; Chapter 3, pp 358–559.

(30) Lee, J.-H.; Bristowe, N. C.; Lee, J. H.; Lee, S.-H.; Bristowe, P. D.; Cheetham, A. K.; Jang, H. M. Resolving the Physical Origin of Octahedral Tilting in Halide Perovskites. *Chem. Mater.* **2016**, *28*, 4259–4266.

(31) Brivio, F.; Walker, A. B.; Walsh, A. Structural and Electronic Properties of Hybrid Perovskites for High-Efficiency Thin-Film Photovoltaics from First-Principles. *APL Mater.* **2013**, *1*, 042111.

(32) Eperon, G. E.; Paternò, G. M.; Sutton, R. J.; Zampetti, A.; Haghighirad, A. A.; Cacialli, F.; Snaith, H. J. Inorganic Caesium Lead Iodide Perovskite Solar Cells. *J. Mater. Chem. A* **2015**, *3*, 19688–19695.

(33) Choi, H.; Jeong, J.; Kim, H.-B.; Kim, S.; Walker, B.; Kim, G.-H.; Kim, J. Y. Cesium-Doped Methylammonium Lead Iodide Perovskite Light Absorber for Hybrid Solar Cells. *Nano Energy* **2014**, *7*, 80 – 85.

(34) Weller, M. T.; Weber, O. J.; Henry, P. F.; Di Pumpo, A. M.; Hansen, T. C. Complete

Structure and Cation Orientation in the Perovskite Photovoltaic Methylammonium Lead Iodide between 100 and 352 K. *Chem. Commun.* **2015**, *51*, 4180–4183.

(35) Glazer, A. M. The Classification of Tilted Octahedra in Perovskites. *Acta Crystallogr., Sect. B: Struct. Sci., Cryst. Eng. Mater.* **1972**, *28*, 3384–3392.

(36) Schiaffino, A.; Stengel, M. Macroscopic Polarization from Antiferrodistortive Cycloids in Ferroelastic $SrTiO_3$. *Phys. Rev. Lett.* **2017**, *119*, 137601.

(37) Kresse, G.; Hafner, J. *Ab Initio* Molecular Dynamics for Liquid Metals. *Phys. Rev. B* **1993**, *47*, 558–561.

(38) Kresse, G. *Ab Initio* Molekular Dynamik für Flüssige Metalle. Ph.D. thesis, Technische Universität Wien, 1993.

(39) Kresse, G.; Furthmüller, J. Efficiency of *Ab-Initio* Total Energy Calculations for Metals and Semiconductors Using a Plane-Wave Basis Set. *Comput. Mater. Sci.* **1996**, *6*, 15 – 50.

(40) Kresse, G.; Furthmüller, J. Efficient Iterative Schemes for *Ab Initio* Total-Energy Calculations using a Plane-Wave Basis Set. *Phys. Rev. B* **1996**, *54*, 11169.

(41) Perdew, J. P.; Ruzsinszky, A.; Csonka, G. I.; Vydrov, O. A.; Scuseria, G. E.; Constantin, L. A.; Zhou, X.; Burke, K. Restoring the Density-Gradient Expansion for Exchange in Solids and Surfaces. *Phys. Rev. Lett.* **2008**, *100*, 136406.

(42) Blöchl, P. E. Projector Augmented-Wave Method. *Phys. Rev. B* **1994**, *50*, 17953–17979.

(43) Kresse, G.; Joubert, D. From Ultrasoft Pseudopotentials to the Projector Augmented-Wave Method. *Phys. Rev. B* **1999**, *59*, 1758–1775.

(44) Monkhorst, H. J.; Pack, J. D. Special Points for Brillouin-Zone Integrations. *Phys. Rev. B* **1976**, *13*, 5188–5192.

(45) Tagantsev, A.; Cross, L. E.; Fousek, J. *Domains in Ferroic Crystals and Thin Films*; Springer-Verlag New York: New York, U.S.A., 2010.

(46) Röhm, H.; Leonhard, T.; Hoffmann, M. J.; Colsmann, A. Ferroelectric Domains in Methylammonium Lead Iodide Perovskite Thin-Films. *Energy Environ. Sci.* **2017**, *10*, 950–955.

(47) Strelcov, E.; Dong, Q.; Li, T.; Chae, J.; Shao, Y.; Deng, Y.; Gruverman, A.; Huang, J.; Centrone, A. CH3NH3PbI3 Perovskites: Ferroelasticity Revealed. *Sci. Adv.* **2017**, *3*.

(48) MacDonald, G. A.; Heveran, C. M.; Yang, M.; Moore, D.; Zhu, K.; Ferguson, V. L.; Killgore, J. P.; DelRio, F. W. Determination of the True Lateral Grain Size in Organic-Inorganic Halide Perovskite Thin Films. *ACS Appl. Mater. Interfaces* **2017**, *9*, 33565–33570.

(49) Hermes, I. M.; Bretschneider, S. A.; Bergmann, V. W.; Li, D.; Klasen, A.; Mars, J.; Tremel, W.; Laquai, F.; Butt, H.-J.; Mezger, M. et al. Ferroelastic Fingerprints in Methylammonium Lead Iodide Perovskite. *J. Phys. Chem. C* **2016**, *120*, 5724–5731.

(50) Govinda, S.; Kore, B. P.; Bokdam, M.; Mahale, P.; Kumar, A.; Pal, S.; Bhattacharyya, B.; Lahnsteiner, J.; Kresse, G.; Franchini, C. et al. Behavior of Methylammonium Dipoles in MAPbX 3 (X = Br and I). *J. Phys. Chem. Lett.* **2017**, 4113–4121.

(51) Yang, M.-M.; Kim, D. J.; Alexe, M. Flexo-Photovoltaic Effect. *Science* **2018**, *360*, 904–907.

(52) Tsai, H.; Asadpour, R.; Blancon, J.-C.; Stoumpos, C. C.; Durand, O.; Strzalka, J. W.; Chen, B.; Verduzco, R.; Ajayan, P. M.; Tretiak, S. et al. Light-Induced Lattice Expansion Leads to High-Efficiency Perovskite Solar Cells. *Science* **2018**, *360*, 67–70.

(53) Jones, T. W.; Osherov, A.; Alsari, M.; Sponseller, M.; Duck, B. C.; Jung, Y.-K.; Settens, C.; Niroui, F.; Brenes, R.; Stan, C. V. et al. Local Strain Heterogeneity Influences

the Optoelectronic Properties of Halide Perovskites. *arXiv preprint arXiv:1803.01192* **2018**,

(54) Viehland, D. D.; Salje, E. K. Domain Boundary-Dominated Systems: Adaptive Structures and Functional Twin Boundaries. *Adv. Phys.* **2014**, *63*, 267–326.

(55) Salje, E.; Zhang, H. Domain Boundary Engineering. *Phase Transitions* **2009**, *82*, 452–469.

(56) Scott, J. F.; Schilling, A.; Rowley, S. E.; Gregg, J. M. Some Current Problems in Perovskite Nano-Ferroelectrics and Multiferroics: Kinetically-Limited Systems of Finite Lateral Size. *Sci. Technol. Adv. Mater.* **2015**, *16*, 036001.

(57) Yang, S. Y.; Seidel, J.; Byrnes, S. J.; Shafer, P.; Yang, C.-H.; Rossell, M. D.; Yu, P.; Chu, Y.-H.; Scott, J. F.; Ager, J. W. et al. Above-Bandgap Voltages from Ferroelectric Photovoltaic Devices. *Nat. Nanotechnol.* **2010**, *5*, 143–147.

(58) Momma, K.; Izumi, F. *VESTA3* for Three-Dimensional Visualization of Crystal, Volumetric and Morphology Data. *J. Appl. Crystallogr.* **2011**, *44*, 1272–1276.